ASME Turbo Expo 2020: Turbomachinery Technical Conference and Exposition,
September 21–25, 2020, Virtual Event, Paper No: GT2020-16336
DOI:10.1115/GT2020-16336

ASSESSMENT OF SURFACE ROUGHNESS EFFECTS ON MICRO AXIAL TURBINES

Abdelaziz A. A. Gamil[1], Theoklis Nikolaidis [1], Joao A. Teixeira [1], S. H. Madani[2], Ali Izadi[2]

[1] Power Engineering Centre, Cranfield University, Bedford, UK
[2] Samad Power Ltd, 9 Centurion Ct, Brick Cl, Kiln Farm, Milton Keynes, UK

ABSTRACT

Surface roughness significantly affects the aerodynamics and heat transfer within micro-scale turbine stages. It results in a considerable increment in the blade profile loss and leads consequently to sizeable performance reductions. The provision of low roughness surfaces in micro gas turbine stages presents challenges on account of the small (mm scale) sizes, manufacturing complexity and associated costs. The axial turbine investigated in this study is fitted to Samad Power's TwinGen domestic micro combined heat and power unit. The micro gas turbine has a compressor pressure ratio of 3, 1200K turbine inlet temperature and a rotational speed of 170,000 rpm. This paper presents a numerical assessment of the effects of varying the surface roughness on the performance and heat transfer of the micro turbine. The surface roughness was uniformly distributed on the NGV and rotor blades. The results showed that increasing the surface roughness from 3 microns to 6, 20, and 100 microns resulted in a reduction in stage total efficiency of 0.8%, 4% and 12% respectively as well as a comparable decrease in output power (0.7%, 3.6%, and 11% respectively). The turbine temperature was also observed to be very sensitive to surface roughness and a temperature increase of some 5% at the rotor hub and over 4% increment in the blade tip surface was observed for 100 microns when compared to the 3 microns surface roughness case. The findings of this paper highlight the adverse effects of the surface roughness on the micro-turbine performance and temperature distribution as well as the importance of careful consideration of wall roughness during the design and manufacturing stages

.

Keywords: Micro Gas Turbine, CFD, surface Roughness, Blade Temperature, Friction Coefficient, Aerodynamic Losses.

NOMENCLATURE

C_f	Friction coefficient
h_s	Sand grain roughness height [m]
h^+	Roughness Reynolds number
k	Von Karman constant
$\dot{m}$	Mass flow rate [Kg/s]
p	Static pressure [Pa]
P_T	Total pressure [Pa]
P_0	Reference total pressure [Pa]
P_{03}	Total pressure at turbine inlet [Pa]
P_{04}	Total pressure at turbine outlet [Pa]
R_a	Arithmetic average roughness [m]
T_0	Reference total temperature [Pa]
u_τ	Friction velocity [m/s]
u^+	Local streamwise velocity [m/s]
V	Free stream velocity [m/s]
y	Distance from the wall [m]
y^+	Non-dimensional distance of the first mesh element
ρ	Density [Kg/m^3]
ε	Diameter of sand-grains sphere [m]
∇	Discrepancy [%]
ΔP	Expansion ration
v	Kinematic viscosity [m^2/s]
τ_ω	local wall shear stress [Pa]
η	Total Efficiency [%]
ζ	Total pressure loss

LIST OF ABBREVIATIONS

CFD	Computational Fluid Dynamics
CO	Carbon monoxide
CO2	Carbon dioxide
H2O	Water vapour
NGV	Nozzle Guide Vanes
PS	Pressure Side
RANS	Reynolds-Averaged Navier–Stokes
rpm	Revolution per minute
SST	Shear stress transport
SS	Suction Side

INTRODUCTION

Surface roughness is an important parameter which can affect the overall performance and aerodynamic losses of the compressors and turbines [1–6]. The efficiency of the turbine is crucial for the gas turbine performance as in some applications a reduction of 1% in the turbine efficiency could result in a 4% reduction in the engine power [7]. Blade surface roughness is one of the design features of the turbines and it can grow considerably (20-150 μm) during the engine operation, especially at high pressure and temperature operating conditions [3,8,9]. A number of methods were used in the literature to examine these effects such as scaling the overall or stage-by-stage performance map of each engine component whilst considering different degradation effects. Another method of examining the degradation and surface roughness effects is to use high-fidelity CFD simulations. This method provides a detailed assessment of the performance and flow distortion in addition to the effect of engine degradation on heat transfer characteristics [10–14].

The consequence of surface roughness on the axial turbines have been investigated in previous studies. A review of the roughness influences on the gas turbines components and an overview of different correlations used to relate the roughness measurements with equivalent sand grains roughness was done by Bons [1]. In addition, the study of non-uniformity of NGV surface roughness by Zhang and Ligrani [15] showed that the aerodynamic loss and wake thickness increased with the increment of surface roughness. Consequently, in the large axial turbines, the surface roughness is usually responsible for a considerable reduction in the overall turbine performance. It can cause about 7% to 14% stage efficiency reduction for roughness values between 0.001 to 0.01 Ks/C as reported by Bammert and Sandstede's [16]. The wall roughness of rotor and NGV has different effects on the overall performance. For a high roughness value (400 μm), the efficiency reduction of the turbine stage was 19% for the fully roughened rotor and NGV compared to the baseline (smooth walls at the rotor and NGV blades). However, the efficiency reduction falls to 8% for a roughened rotor and 11% for roughened NGV [17]. In addition, Kang et al. [18] investigated numerically the effects of transitional and fully rough regimes (equivalent sand-grain roughness of 100 and 400 μm) on a low-speed turbine performance. They found that the output work reduction occurred because of the surface roughness increment. They also reported that for both surface roughnesses, the model was more sensitive the NGV roughness and it caused an additional 10% reduction in the turbine work compared to the stage rotor.

Some of the turbine flow parameters such as the Reynolds Number can be directly linked with the performance degradation due to wall roughness [19,20]. These effects become more significant on the boundary layer and remarkably increase the aerodynamic losses at high Reynold numbers [21–23]. The effects of wall roughness on the turbine performance at different Reynolds numbers is more obvious compared to its influence on the turbulence intensity levels at the stage inlet [24,25]. Furthermore, the aerodynamic losses were found to be also sensitive to the location of the roughened surface. The experimental measurement of Kind et al. [26] of roughness effects on a turbine cascade indicated that roughness values had a relatively small influence on the blade pressure coefficient and flow deviation angle. However, the small change in deviation angle can result in a considerable amount of reduction in the turbine work [18]. The wall roughness on the blade suction side walls also found to have a stronger effect on the flow losses than equivalent roughness on the pressure side surface. For instance, in transonic compressors, the wall roughness at the blade leading edge and the upstream part of the suction side were responsible for approximately 70% of the efficiency reduction as reported by Suder et al. [27].

Furthermore, for gas turbine engines, it is crucial to accurately estimate the thermal loads on the turbine stage, as it is an important factor for assessment of the engine life and durability. The turbine passage surface roughness changes the spanwise flow distribution and therefore the heat transfer ratio within the turbine. The experimental study of Blair [28,29] on a large scale rotor indicated that the increment of surface roughness from smooth to rough (Rz roughness between 8 to 84 mm) caused a two-fold increase in the model heat transfer. Furthermore, Lorenz et al. [30] investigated the heat transfer process in a turbine cascade for a range of surface roughnesses (equivalent sand grain roughness 120 to 290 mm), Reynolds numbers ($5*10^4$ to $25*10^4$), and inlet turbulence intensities (1 to 10%). The results showed that the increment of Reynolds number improved the heat transfer inside the turbine and that the high roughness case increased the heat transfer by 100%. A numerical investigation of NGV endwall roughness on the heat transfer was carried out by E. Lutum et al. [31]. They found that the heat transfer of the endwall significantly increased by applying the surface roughness. This result agreed with the numerical investigation of the heat transfer coefficient of turbine NGV with rough surface roughness conducted by Guo et al. [32]. The roughness of turbine surfaces is usually one of the design specifications and it can directly affect the production cost. Previous publications have highlighted the roughness effects on the prevailing scale turbines, however, no studies were found on the

roughness influences on the micro-scale axial turbines and limited information are available in this scale. Due to the high surface to volume ratio in a micro gas turbine, the roughness effects are anticipated to be pronounced. This paper reports the numerical investigation of the effect of surface roughness on the performance, aerodynamic loss, and temperature distribution of a microscale turbine. This paper provides a validated case with experimental data and discuss in details the effects of surface roughness on a micro turbine stage. The numerical simulations were carried out using the commercial code ANSYS CFX 19.1 and the CFD models and results were verified and validated against experimental data.

TURBINE GEOMETRY

The device simulated in this paper was a micro axial turbine used in the TwinGen [33] engine which represents an innovative, compact, and high-performance CHP system for domestic use. The micro gas turbines power generation units which can provide 25 to 500 KW of power. The TwinGen unit was designed to provide 18kW of heat and 2kW of electrical power with an overall system efficiency of up to 93%. The engine has a low mass flow rate (26 – 27g/s) and a high rotating speed (170,000 rpm). The turbomachinery components are a radial compressor and a single-stage axial turbine. The axial turbine was designed by Cranfield University for the TwinGen gas turbine to provide about 6 kW power. The turbine has a very low aspect ratio, as shown in Fig. 1, on account of the low flow rate and high rotation speed of the unit. The inlet conditions of the turbine were a total pressure of 273kPa and a total temperature of 1200K with the exhaust gases, discharged with a total pressure close to the ambient conditions (103 KPa), being directed onto a heat exchanger using the outlet duct. . The geometrical details of the axial turbine are presented in Table 1.

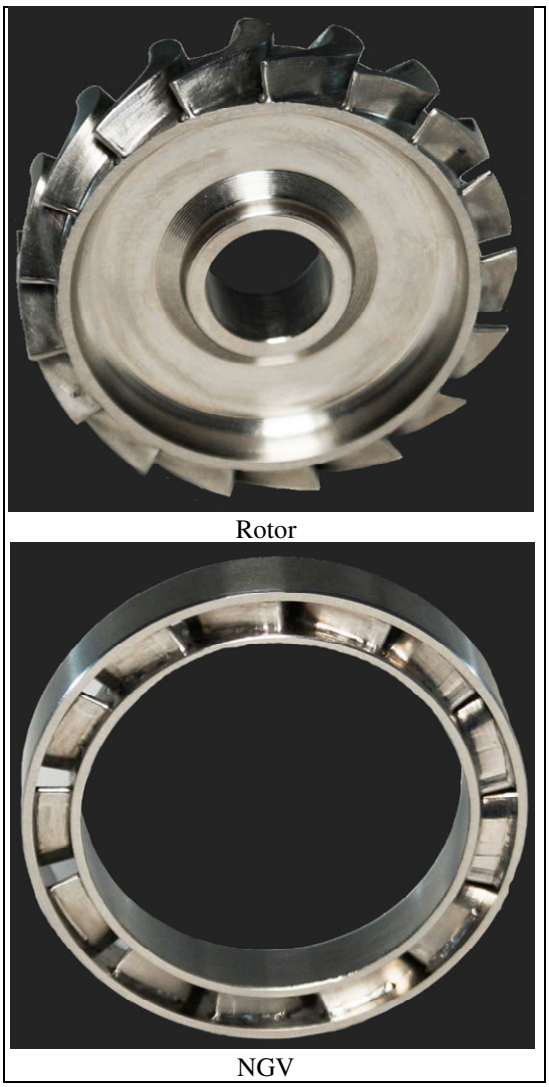

Figure 1: Geometry of TwinGen Turbine

Table 1: Design Parameters

	NGV	Rotor
Hub diameter (mm)	37	37
Tip diameter (mm)	44	44
Number of blades	13	17
Axial cord (mm)	4.8	8.6
Blade pitch at avg. diameter (mm)	10	7.5
Leading edge diameter (mm)	1.2	1.2
Trailing edge diameter (mm)	0.8	0.8
Inlet metal angle (degrees)	0	46
Outlet metal angle (degrees)	78	68

NUMERICAL MODELLING

In this study, the numerical simulations were performed using ANSYS CFX 19.1 commercial code. The numerical solution was obtained by solving the Reynolds-Averaged Navier-Stokes equations (RANS) using the finite volume method to solve the flow model. The numerical results were obtained by running steady-state simulations which included the energy equation accounting for the viscous work. High-resolution advection scheme and turbulence numerics were used to obtain the numerical solution.

The Shear Stress Transport (SST) turbulence model was selected because it was originally developed to provide an improved prediction of the flow in regions of adverse pressure gradient and separation. In the SST model, the turbulence viscosity is adjusted to consider the transport of the principal flow shear stress. This turbulence model combines the k-ε and k-ω models where and k-ω is used near the walls while k-ε is used in the free stream region. The SST model has been enhanced within the ANSYS-CFX code, and the model near-wall formulation decreases the requirements of grid resolution near walls [34].

The wall roughness has significant influence on the flow structure and losses in the turbine. The surface roughness increases the near wall turbulence and consequently, affects the shear stresses and changes the rate of heat transfer through the turbine elements. In fact, in turbulent flow, the roughened walls promote not only increase the wall shear stress but also the separation of the viscous sublayer. Therefore, the accuracy of the results is intimately related to the accurate modelling of the wall roughness. The roughness effects can be activated in CFX and modelled by including a downstream shift in the logarithmic velocity profile equation (equation 1). This downstream shift (equation 2) is a function of the dimensionless value of the roughness height and for the sand grain roughness which can be calculated using equation 3 [31,35–37].

$$u^+ = \frac{1}{k} ln(y^+) + B - \Delta B \tag{1}$$

$$\Delta B = \frac{1}{k} ln(1 + 0.3h^+) \tag{2}$$

$$h^+ = \frac{h_s u_\tau}{\nu} \tag{3}$$

Where B = 5.2 and y^+ is the non-dimensional distance of the first mesh element from the walls and h_s is the sand grain roughness. Based on the value of sand grain roughness, three regions can be identified in the model. If h_s is less than 5 then the walls can be considered as hydraulically smooth; if the value of h_s is greater than 5 but less than 70, then the case is classified as intermediate roughness. When the roughness exceeds 70 then the wall is classified as fully rough. The near wall model setup was set to automatically allow the code to select either the wall function or low Reynolds formulations depending on the grid element resolution near the wall.

A number of parameters have been used to quantify the surface roughness such as the arithmetic average, root mean square, and root to valley values. In the current study, the arithmetic average values were employed due to the availability of this information and since it can be calculated using equation (4) [38].

$$R_a = \frac{1}{n} \sum_{i=1}^{n} |y_i| \tag{4}$$

In this study, four values of roughness R_a (3, 6, 20, and 100 microns) were examined as a reflection on the expected surface roughnesses of different manufacturing techniques. These values cannot be applied directly to the CFD setup as the sand grain roughness, which is commonly used to predict the wall friction coefficient from the Moody diagram, does not directly represent any type of surface roughness measurements. As a consequence using the measured value of surface roughness as sand grain roughness can result in substantial errors in estimating roughness effects in turbomachinery flows and performance [38]. Conversion algorithms have been proposed in a number of studies to convert different roughness measurements to san grains values as shown in equation 5. Analytical models are used to relate this equation to the diameter of the sand grain spheres (ε), resulting in the estimation sand-grain equivalent roughness as shown in equation (6). Based on experimental results, the estimated sand-grain roughness using equation (6) has shown good results as an approximation of the roughness values [38].

$$R_a = \frac{1}{\varepsilon}\int_{x=0}^{\varepsilon} |y - \bar{y}|\, dx. \quad (5)$$

$$\varepsilon = 5.863 R_a \quad (6)$$

The parameters used to assess the numerical results are total pressure loss, normalized helicity and friction coefficient. The total pressure coefficient which indicates the pressure losses within the turbine can be expressed as

$$\zeta = \frac{P_{T,i} - P_T}{\frac{1}{2}\rho_i V_i^2} \quad (7)$$

The pressure coefficient distribution around the blade is associated with the rotor work coefficient and is defined as

$$C_P = \frac{p_i - p_T}{\frac{1}{2}\rho_i V_i^2} \quad (8)$$

Friction coefficient represents the non-dimensional value of the local surface shear stress and it describes the flow conditions near the model walls. The friction coefficient can be expressed as

$$\mathrm{C_f} = \frac{\tau_\omega}{\frac{1}{2}\rho V^2} \quad (9)$$

The boundary conditions were assigned as follow. The computational fluid domain contained one NGV blade and one rotor blade in addition to a sector of the outlet duct which represents a quarter of the outflow duct. Periodic conditions in the circumferential direction about the z-axis were assigned to the NGV, rotor, and outlet sections. Total pressure and temperatures, as well as the direction of the flow, were assigned to fluid domain inlet which was located upstream of the blade 1.5 times the averaged axial chord distance of the NGV. The flow turbulence intensity at the inlet was 5%. Static pressure was specified at the exit of the outlet duct averaged over the whole outlet with a profile blending factor of 0.05. The rotor hub and blades were specified as a rotating wall in a fixed reference frame with the no-slip condition. The shroud was specified as in a counter-rotating wall in a relative reference frame with the no-slip condition. For the model validation, the numerical simulations were performed for different expansion ratios (1.06, 1.18, 1.38, 1.58, 1.83) and rotational speeds of 150,000 RPM. The working fluid in the turbine is made up of the combustor exhaust gases flow containing a mixture of CO2, H2O, N2, and O2 gases. The surface roughness was applied to the various walls of the fluid domain, hubs, shrouds, stationary and rotating blades.

Four cases were created to examine the dependency of the computational model on the number of grid elements. These cases have 0.5, 1, 2, and 4 million nodes as shown in Table 2. The results show that the numerical model becomes nearly grid independent when it exceeds 2 million nodes. The discrepancy between the total efficiency and expansion ratios of the 2 and 4 million cases was about 0.08% and 0.002% respectively. Based on these results, the mesh of the fluid domain of the turbine stage was finalised as follows. A structured mesh was generated in the NGV, rotor and outlet domains as shown in Fig. 2. A H-grid type was used in the flow passage, while an O-grid type was used around the rotor and NGV blades to improve the overall mesh quality and the accuracy of the results. The thickness of the O-grid layer around the blade was 30% of the average blade thickness and consisted of 30 grid nodes with non-dimensional y+ less than one. The expansion ratio of the grid elements in all directions was set at 1.1. The total number of grid nodes of the NGV and rotor computational domains was approximately 2,300,000, while the outlet duct had 400,000 nodes. Overall, the grid resolution of the model was fine with the *y+* values near the walls (such as 50% of rotor blade span) being lower than 0.3 as shown in Fig. 3.

Table 2: Mesh Dependency Study

Grid No.	η	∇	$\Delta \boldsymbol{P}$	∇
500,000	78.24%	-	2.6832	-
1,000,000	76.34%	2.43%	2.6864	0.121%
2,000,000	76.27%	0.09%	2.6863	0.005%
4,000,000	76.21%	0.07%	2.6862	0.002%
	NGV		Rotor	

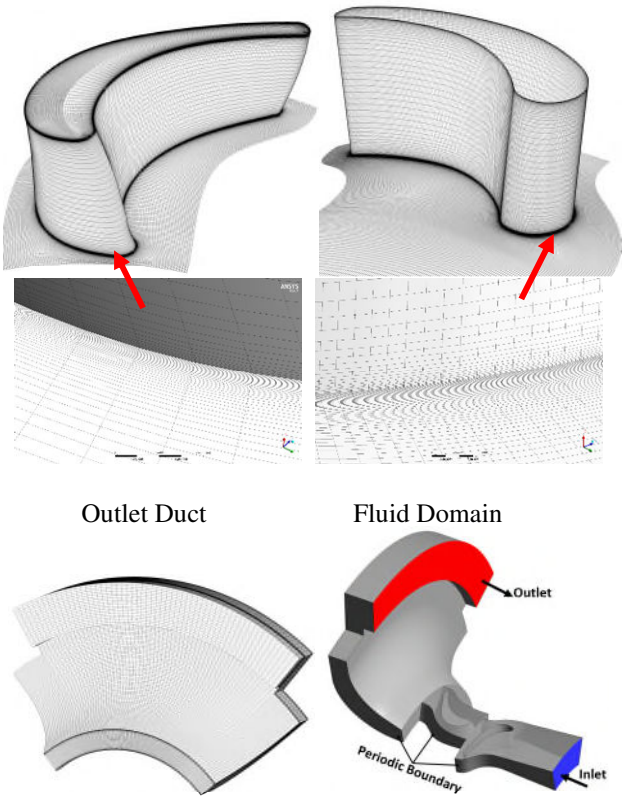

Figure 2: Grid of CFD Domains

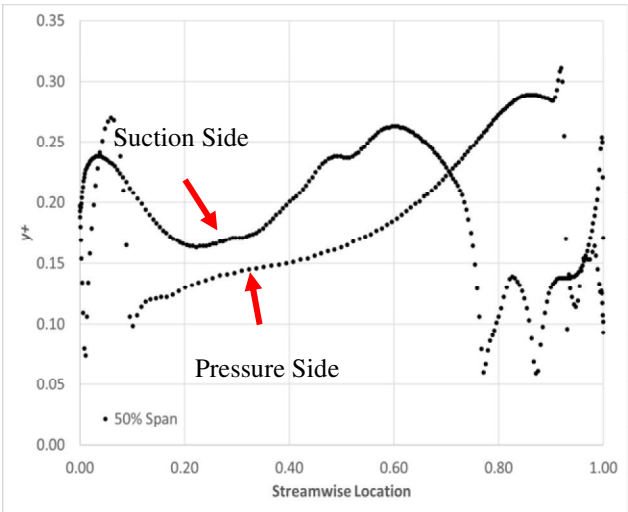

Figure 3: y+ at 50% of Rotor Blade Span

VALIDATION

The numerical model was validated with experimental data. Samad Power Ltd. provided the experimental results of the turbine stage after conducting different test runs and measurements. The test rig used to obtain the performance measurements for the TwinGen engine and a schematic representation of the experimental setup are shown in Fig.4 and Fig. 5. The following parameters were extracted from the experimental data to establish the turbine characteristic map.

1- Turbine mass flow, $\dot{m}$
2- Turbine inlet pressure, P_{03}
3- Turbine inlet temperature, T_{03}

4- Turbine outlet pressure, P_{04}

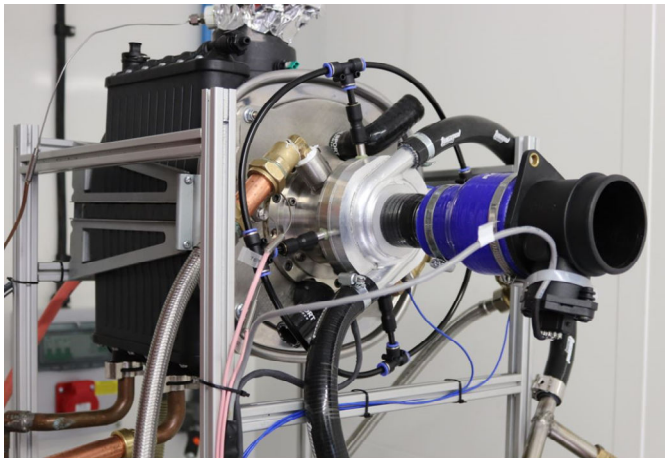

Figure 4: Experimental Test Rig

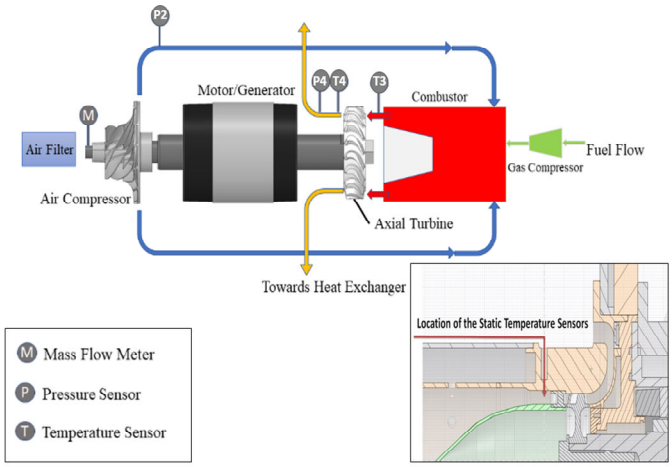

Figure 5: TwinGen test bench layout

All pressures and temperatures were measured in the static form and their total corresponding was calculated by considering the air mass flow rate and the relevant cross section area. Pressure was measured in the compressor outlet and considering around 3% pressure drop in the combustion chamber to calculate the turbine inlet pressure. The static temperature was measured in various angles exactly before the turbine NGV and the Turbine inlet temperature was the average of these readings.

- In all measurements, the pressure sensors accuracy was around 0.25%. For instance, for the pressure measurement of 200kPa, the sensor accuracy was around $\pm 0.5\ kPa$.
- The Temperature sensors were K-type to withstand in the high temperature environment and their accuracy linearly depend on the measured temperature by: ±0.004T (350-1100℃). For example, in the 1200K, 926.85 ℃, its accuracy is around ±3.7℃

In the testing data, the uncertainties of the variables used for the turbine inlet corrected mass flow and expansion ratio were considered as follow.

- For the turbine Inlet corrected mass flow rate, the TIT or T03 was the averaged value of the static temperature at 5 different angle corresponding to various regions of the fluid at the turbine inlet annulus, considering the periodic effects and angles of the fuel inlet nozzles inside the combustion chamber. In addition, by calculating the flow velocity at the mid-radius of the annulus, the total temperatures have been calculated.
- For the turbine expansion ratio, uncertainty was related to the calculation of total pressure using the measurement of static pressure at the compressor outlet and turbine outlet. The turbine total inlet pressure was calculated by adding the dynamic pressure to the static pressure at the outlet of compressor considering the combustion chamber pressure loss.

These parameters were used to calculate the turbine expansion ratio and the corrected mass flow using the following equations.

$$Corrected\ Mass\ Flow = \frac{\dot{m}\sqrt{T_{03}}}{P_{03}} \tag{10}$$

$$Turbine\ Expansion\ Ratio = \frac{P_{03}}{P_{04}} \tag{11}$$

The numerical results were validated against experimental data for different expansion ratios as shown in Fig. 6. The testing data were limited to an expansion ratio of about 1.8 and a rotational speed of 150,000 rpm due to the test rig limitations The turbine, compressor and motor/generator were on the same shaft, therefore, motor/generator acting as a dynamic load on the turbine. The TwinGen unit was governed by motor/generator to control the speed and fuel flow to control the Turbine inlet temperature. Using these two types of controller it was possible to test the turbine and compressor matching at various off design point.. The simulation is conducted in the same rotational speed but as it was already investigated and proved by gas turbine performance scholars, the turbine map is relatively independent from the rotational speed. In other word, each point in the curve can be calculate from different specific speed which correspond to speed of machine in some off-design points. The numerical results were obtained for the model with 3µm Ra roughness similar to the measured surface roughness of the tested turbine. The performance curve of the numerical results showed a similar trend when compared to the experimental data and the CFD results agreed well with the experimental data. Although the testing data were limited in terms of shaft rpm, the agreement between the numerical results and the measurements indicate that the numerical model can accurately predict the performance of the axial turbine for different operating conditions.

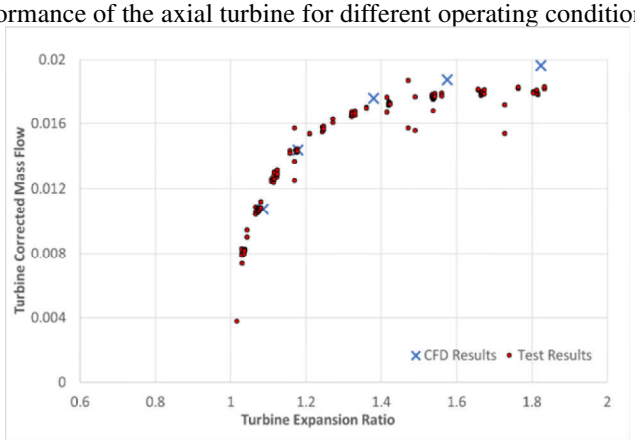

Figure 6: Corrected Mass Flow versus Expansion Ratio

RESULTS AND DISCUSSION

The power and efficiency of the axial turbine with different roughness values are shown in Table 3. The results were obtained by applying three different surface roughnesses to the NGV and rotor walls. All simulations were conducted at the design point (273kPa and 1200K turbine inlet total pressure and temperature and 170,000 rpm). The results show that both turbine power and efficiency decrease as the surface roughness increases. The turbine efficiency was slightly more sensitive to the increment of surface roughness when compared to the power. In the presence of surface roughness, the profile drag rises as a result of boundary layer thickness growth and therefore the turbine efficiency drops. In this paper, the 3 µm case was considered as the baseline for all comparisons because it had similar surface roughness to the tested turbine and it was validated with the testing data. Between the 3 and 6 micron models about 0.7% and 0.8% reductions in power and efficiency have occurred. However, significant performance reductions were predicted as a result of high surface roughness (100 µm) and the turbine lost 11% of the power and 12% of the total efficiency. The results indicated that a small performance reduction happens in the case of 6µm, and then the performance degradation dramatically increases in the case of 20 microns. Although, the surface roughness had significant effects on the performance, the turbine designers might accept the performance degradation and select high roughness manufacturing techniques due to technological limitations and budget requirements. The results indicate that the efficiency reduction in micro gas turbines with a roughness of 100µm (12%) was relatively minor when compared to an efficiency reduction in a full scale turbine estimated by Yun et al. [17], to be 19% for a rotor and NGV surface roughness of 400µm.

Table 3: Turbine Performance with Surface Roughness

Model	Roughness Ra (µm)	η %	∇ %	Power (kW)	∇ %
3 Ra	3	76.5	-	6	-
6 Ra	6	75.9	0.8	5.96	0.7
20 Ra	20	73.3	4.2	5.79	3.6
100 Ra	100	67.4	11.9	5.34	11.0

The effect of the surface roughness on the wake region of the NGV and rotor blades is shown in Fig. 7. The mass average of the relative velocity at mid-span was plotted against the pitch-wise location. The results show that for the rotor and NGV, the size and depth of the wake zone increases as the roughness value increases. The profile loss generated due to the roughness increment near the trailing edge at the blade suction side was the reason for the wake increase as stated by Kang et al [35]. The effect of the roughness was less significant in the case of the rotor when compared to the NGV due to the high turning of the stationary blades. For a surface roughness greater than 6 microns, the wake downstream of the NGV blade widened significantly and the flow velocity considerably decreased especially in the case of 100 microns roughness. The size and velocity magnitude in the NGV wake affect the location of the stagnation point in the rotor. Consequently, the pressure distribution of the rotor blades will be changed and therefore affect the turbine power and efficiency. For the rotor blade, a small shift of the centre of the wake zone towards the blade suction side occurred as a result of surface roughness increment. However, for the wake of the NGV blades, the core of the wake zone was changed and the wake area was noticeably shifted towards the blade suction side surface. The effect of the surface roughness on the wake regions has negative impacts on the performance of the axial turbine.

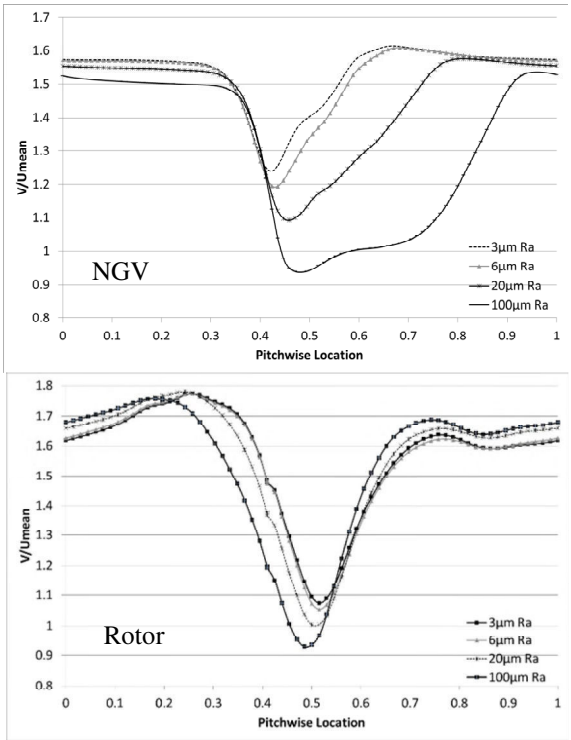

Figure 7: NGV and Rotor Blade Wake

The friction coefficient (Fig. 8) was used to highlight the effects of roughness on the wall shear stress and therefore, the blade profile loss. It can also be used to highlight the flow separation point and the size of the separation bubble. The friction coefficient at the pressure side was sensitive to the surface roughness when compared to the blade suction-side surface. For the blade pressure side, the effect of roughness was minimal between the leading edge and 70% of the axial chord, after which the friction coefficient increases significantly until the blade trailing edge. However, for the suction side surface, the friction coefficient increased gradually from the leading edge and reached the peak value at approximately 70% of the streamwise location. The peak region of the friction coefficient distribution at the blade suction surface represents an indication of flow separation from the blade wall. Therefore, as the friction coefficient increase, the flow separation zone and its associated losses increases. The friction coefficient curve was almost identical in the case of 6 microns when compared to the 3µm surface roughness. The friction coefficient increases significantly in the case of 20 and 100µm roughness, and the peak value at the blade suction side jumped respectively by 70% and 190% when compared to the 3 microns model.

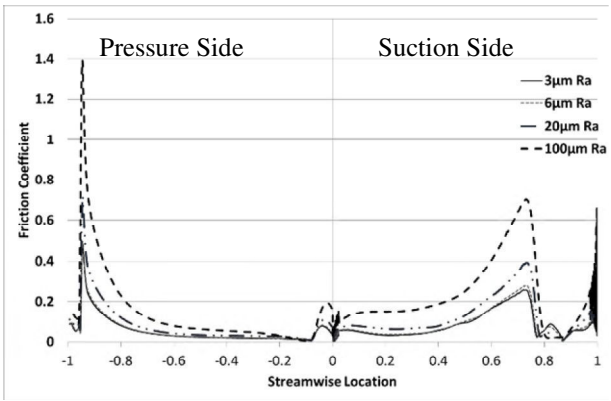

Figure 8: Rotor Friction Coefficient

The loss in total pressure will directly affect the total efficiency of the axial turbine and consequently, the overall engine performance will be negatively affected. The mass flow averaged total pressure coefficients between the hub and shroud at the rotor outlet are shown in Fig. 9. The total pressure loss increases as the roughness increase as a result of blade profile loss growth [9]. In general, the total pressure coefficient of 3 and 6 microns were very similar, especially near the blade mid-span. The total pressure loss of the 20 microns model became more noticeable between 60% to 90% of the blade span when compared to the 3 microns turbine. Furthermore, the total pressure loss increases remarkably in the case of the 100µm surface roughness model which indicates a considerable increase in the flow aerodynamic losses. The averaged total pressure loss along the span increased respectively by 2% and 6.5% for the 20 and 100 µm models when compared to the 3 microns turbine.

The turbine work coefficient is associated with the distribution of pressure coefficient in the rotor blade (loading). Fig. 10 shows the distribution of the pressure coefficient at the mid-span of the rotor blade. The increase in surface roughness generally caused a reduction in the pressure coefficient distribution in both suction and pressure surfaces and consequently a higher-pressure coefficient difference along the rotating blades. The pressure distribution of 6 micron model was almost similar to the 3 micron case while the 20 micron surface roughness model was had a small deviation compared to the 3 µm model. The effect of the surface roughness on the blade pressure distribution was relatively significant in the case of 100 microns. The effect of the surface roughness was more noticeable at the pressure side surface between the leading edge and about 70% of the stream-wise distance. Between 70% of the axial chord and the trailing edge, the surface roughness value significantly affects the pressure distribution of the suction side surface. In fact, the pressure coefficient decreased with the increment of surface roughness resulting in a higher pressure difference between the blade suction and pressure sides and consequently a higher flow deviation angle as stated by [18,35]. The reduction of the pressure coefficient at the suction side near the blade trailing edge was a result of the total pressure loss increment. The roughness value of the NGV affected the upstream flow conditions and the deviation angle and therefore, it also affected the blade loading. However, a detailed evaluation of the NGV roughness and its influences on the downstream flow structure will be investigated in a future work.

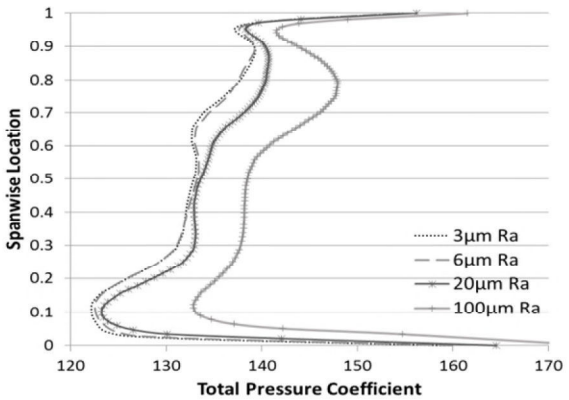

Figure 9: Rotor Total Pressure Coefficient

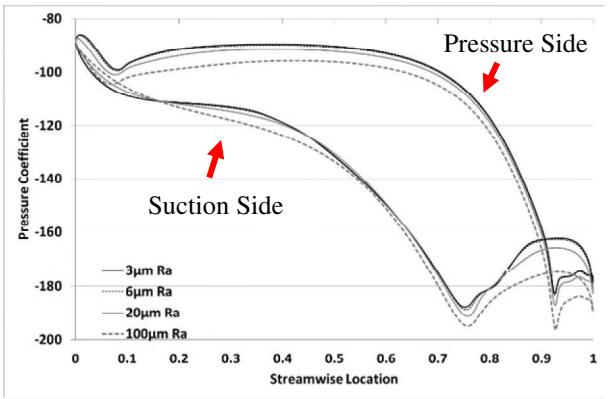

Figure 10: Rotor Pressure Coefficient Distribution

The temperature distributions of the mid-span of the rotor blade at the pressure and suction sides are shown in Fig. 11. In the pressure side surface, the temperature profiles of 3 and 6 micron models showed a gradual temperature increase between 50% of the blade chord and the trailing edge. The temperature increment at the aft part of the blade with 3 and 6 microns exceeded the temperature values at the blade surface of the 20 and 100 µm turbines. The 100 microns surface roughness resulted in an approximately 2% higher blade temperature except for the region between 80% of the blade chord and the trailing edge. Furthermore, the temperature distribution of the 3, 6, and 20 micron models showed two peaks along the suction side surface. The first peak had almost similar temperature values for the three models and were shifted slightly downstream of the blade as the roughness value increased. For instance, the first temperature profile peak of the 20µm case was located at 45% of the blade chord, while the same region occurred at 35% of the chord in the 3 micron model. In addition, the second peak of the temperature profile was located at about 75% of the blade chord and it had a significant reduction in the temperature magnitude as the surface roughness increased. Moreover, for the 100 micron turbine, the temperature distribution of the suction side surface had one peak and was higher than the other roughness models until 30% of the blade chord. The temperature profile peak of the 100µm case was located approximately 57% of the blade chord. However, the magnitude of the temperature in this region did not change noticeably compared to other models. The shape and magnitude of the temperature profiles and locations of the peaks were related to the location of the stagnation point and the acceleration of the flow around the blade surface and the existence of flow separations near the blade walls. The temperature profiles shown in Fig. 11 identified the location of the hot spots on the blade material and the effects of the roughness on the temperature distribution. These results are important for the structural and thermal analysis and the design of blade cooling methods that will be discussed in the future publication.

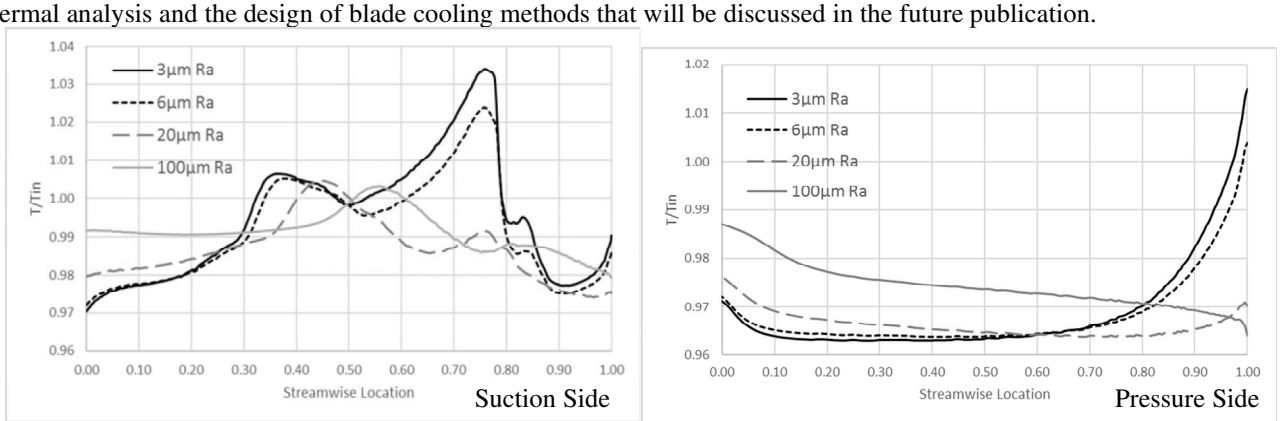

Figure 11: Rotor Temperature Distribution

The blade tip region is very sensitive as it is exposed to high-temperature flows. This has a direct effect on the turbine stage thermal stresses and therefore on the durability of the engine. The effect of the blade roughness on the temperature profile at the tip region (Fig. 12) indicated that the tip region has a similar structure of temperature distribution for different models with a maximum temperature spot located about 60% of the blade chord near the suction-side surface. However, the maximum temperature zone slightly increased with the increment of the roughness. For the 3 micron case, the maximum temperature spot was about 1700K and it was increased by 0.6%, 2%, and 4% in the case of 6 and 20, and 100 microns respectively. The difference in maximum temperature values was due to the change of leakage flow structure and magnitude due to the presence of the surface roughness. The temperature distribution will adversely affect the blade material near the suction side and the blade trailing edge, which might lead to large metal expansion and increase the

possibility of damage to the blade. Therefore, the increment of 4% in the tip region temperature should be examined during the design and manufacturing phases and a cooling method can be implemented to overcome the negative consequences. The turbine designers can select also different materials for the turbine stage however, this might increase the manufacturing cost of the unit.

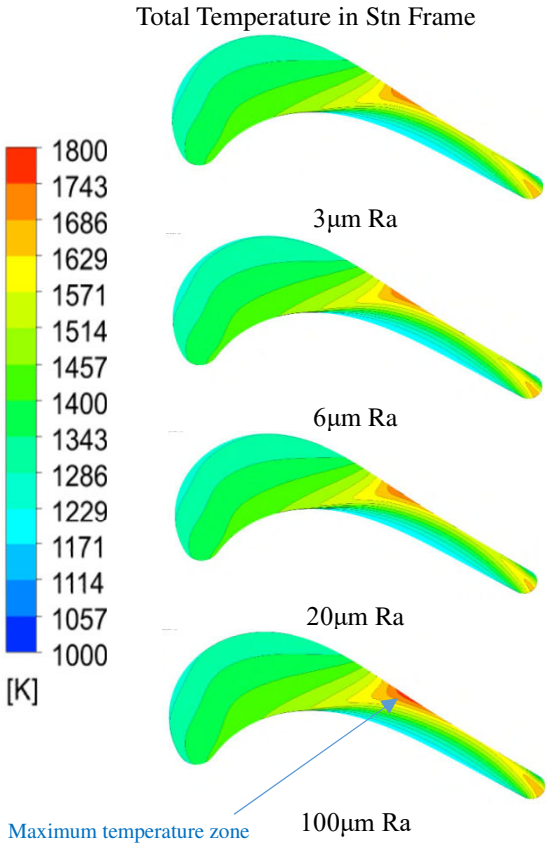

Figure 12: Rotor Tip Temperature

The effect of surface roughness on the rotor hub was also investigated. This area is subject to the peak mechanical stresses and the temperature profile on the hub region will cause additional thermal loads on the turbine rotor. The increment of thermal stresses on the hub region affects the durability of the turbine stage and increases the possibility of engine failure. The temperature profile of the rotor hub (Fig. 13) shows that the high surface roughness increased the temperature of the hub surface. This effect can be seen near the leading edge at the blade suction side area and at the downstream blade to blade passage. For instance, in the case of 100 microns roughness, the temperature near the blade leading edge and at the downstream passage increased by 4% and 5% respectively compared to the 3 micron surface roughness model.

Based on these results, it is clear that the current turbine stage should be manufactured with very low surface roughness to reduce the possibility of damage to the blade; alternatively, some cooling methods should be applied to cool down the tip region of the rotating blades.

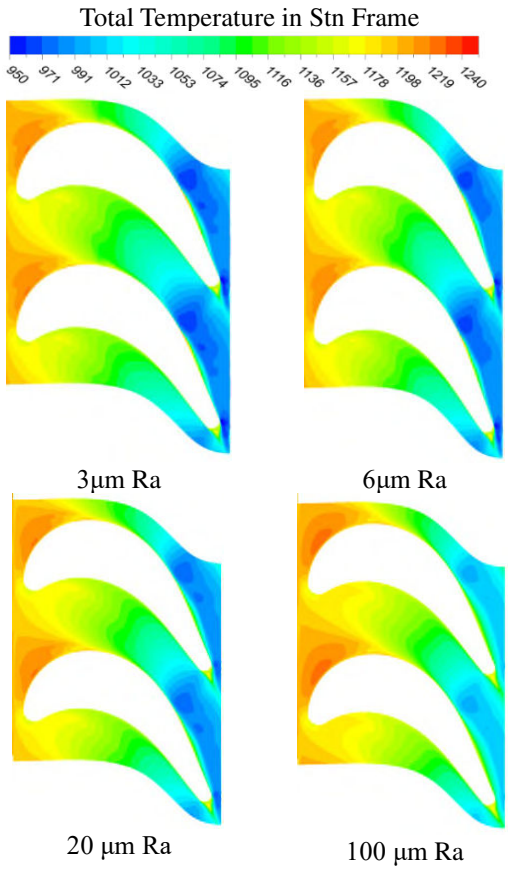

Figure 13: Rotor Hub Temperature

CONCLUSION

The level of surface roughness and manufacturing tolerances affects the production time and cost of gas turbine engines. In this paper, the influences of surface roughness TwinGen micro axial turbine to address the manufacturing cost issues associated with the unit production, as it was difficult to meet the required roughness (3 microns) without additional manufacturing processes. The specific effect of the roughness value on the performance of the micro-turbine stage has not been covered previously. This paper investigated numerically the influences of four surface roughnesess (3, 6, 20, and, 100µm Ra) on the micro-turbine aerodynamics and temperature distribution. The main findings of this research were:

- The turbine performance decreased essentially linearly with the surface roughness increment.
- The turbine power and efficiency dropped by 11% and 12% respectively as the roughness increased from 3 to 100 microns.
- The surface roughness considerably increased the blade's wake zones and the total pressure losses.
- The effects of rotor roughness on the blade pressure distribution were less obvious in the suction-side surface compared to the pressure-side except near the trailing edge.
- The blade tip temperature respectively increased by 0.6%, 2%, and 4% for the 6, 20, and 100 microns roughness compared to the 3µm model.
- The rotor hub region was also sensitive to the roughness increment and the temperature roughly rose only by 2.7% and 5% for 20 and 100 microns compared to the baseline model (3µm).

The findings of this paper illustrate the influences of the surface roughness on TwinGen micro-turbines and the significant aerodynamic losses and temperature increment it can cause. Based on the current research findings, TwinGen turbine should not be manufactured with surface roughness more than 6 microns; otherwise, significant performance penalties can take place. The conjugate heat transfer analysis will be carried out in future publications to provide a detailed assessment of the internal metal temperature of the NGV and rotor blades.

ACKNOWLEDGEMENTS

The authors wish to acknowledge the financial support for this work from Innovate UK. Finally, we would like to thank SAMAD Power Ltd for the permission to present this material.

REFERENCES

[1] Bons, J. P., 2010, "A Review of Surface Roughness Effects in Gas Turbines," J. Turbomach., **132**(2), p. 021004.

[2] Morini, M., Pinelli, M., Spina, P. R., and Venturini, M., 2011, "Numerical Analysis of the Effects of Nonuniform Surface Roughness on Compressor Stage Performance," J. Eng. Gas Turbines Power, **133**(7), p. 072402.

[3] Tarada, F., and Suzuki, M., 1993, "External Heat Transfer Enhancement to Turbine Blading due to Surface Roughness," International Gas Turbine and Aeroengine Congress and Exposition, American Society of Mechanical Engineers.

[4] Taylor, R. P., 1990, "Surface Roughness Measurements on Gas Turbine Blades," J. Turbomach., **112**(2), p. 175.

[5] Bogard, D. G., Schmidt, D. L., and Tabbita, M., 1998, "Characterization and Laboratory Simulation of Turbine Airfoil Surface Roughness and Associated Heat Transfer," J. Turbomach., **120**(2), p. 337.

[6] Bons, J. P., Taylor, R. P., McClain, S. T., and Rivir, R. B., 2001, "The Many Faces of Turbine Surface Roughness," J. Turbomach., **123**(4), p. 739.

[7] Diakunchak, I. S., 1992, "Performance Deterioration in Industrial Gas Turbines," J. Eng. Gas Turbines Power, **114**(2), pp. 161–168.

[8] Bai, T., Liu, J., Zhang, W., and Zou, Z., 2014, "Effect of surface roughness on the aerodynamic performance of turbine blade cascade," Propuls. Power Res., **3**(2), pp. 82–89.

[9] Aligoodarz, M. R., and Derakhshan, F. E., 2013, "Numerical study of blade deterioration effects on an industrial gas turbine stage performance and flow field," Proc. Inst. Mech. Eng. Part A J. Power Energy, **227**(4), pp. 515–527.

[10] Bettocchi, R., and Spina, P. R., 1999, "Diagnosis of Gas Turbine Operating Conditions by Means of the Inverse Cycle Calculation," Volume 2: Coal, Biomass and Alternative Fuels; Combustion and Fuels; Oil and Gas Applications; Cycle Innovations, American Society of Mechanical Engineers.

[11] Gulati, A., Zedda, M., and Singh, R., 2000, "Gas turbine engine and sensor multiple operating point analysis using optimization techniques," 36th AIAA/ASME/SAE/ASEE Joint Propulsion Conference and Exhibit, American Institute of Aeronautics and Astronautics, Reston, Virigina.

[12] Lakshminarasimha, A. N., Boyce, M. P., and Meher-Homji, C. B., 1994, "Modeling and Analysis of Gas Turbine Performance Deterioration," J. Eng. Gas Turbines Power, **116**(1), p. 46.

[13] Morini, M., Pinelli, M., Spina, P. R., and Venturini, M., 2008, "Influence of Blade Deterioration on Compressor and Turbine Performance," Volume 7: Education; Industrial and Cogeneration; Marine; Oil and Gas Applications, ASME, pp. 505–516.

[14] Morini, M., Pinelli, M., Spina, P. R., and Venturini, M., 2009, "CFD Simulation of Fouling on Axial Compressor Stages," Volume 5: Microturbines and Small Turbomachinery; Oil and Gas Applications, ASME, pp. 331–342.

[15] Zhang, Q., and Ligrani, P. M., 2006, "Aerodynamic Losses of a Cambered Turbine Vane: Influences of Surface Roughness and Freestream Turbulence Intensity," J. Turbomach., **128**(3), p. 536.

[16] Bammert, K., and Sandstede, H., 1980, "Measurements of the Boundary Layer Development along a Turbine Blade with Rough Surfaces," J. Eng. Power, **102**(4), p. 978.

[17] Yun, Y. Il, Park, I. Y., and Song, S. J., 2005, "Performance Degradation due to Blade Surface Roughness in a Single-Stage Axial Turbine," J. Turbomach., **127**(1), p. 137.

[18] Kang, S., Kang, Y., and Han, K., 2003, "Numerical Study on Blade Roughness Effect on the performance of turbomachines," Proc. Int. Gas ….

[19] Boyle, R. J., 1994, "Prediction of Surface Roughness and Incidence Effects on Turbine Performance," J. Turbomach., **116**(4), pp. 745–751.

[20] Boyle, R. J., and Senyitko, R. G., 2003, "Measurements and Predictions of Surface Roughness Effects on the Turbine Vane Aerodynamics," Volume 6: Turbo Expo 2003, Parts A and B, ASME, pp. 291–303.

[21] Denton, J. D., 1993, "Loss Mechanisms in Turbomachines," Volume 2: Combustion and Fuels; Oil and Gas Applications; Cycle Innovations; Heat Transfer; Electric Power; Industrial and Cogeneration; Ceramics; Structures and Dynamics; Controls, Diagnostics and Instrumentation; IGTI Scholar Award, ASME, p. V002T14A001.

[22] Montis, M., Niehuis, R., and Fiala, A., 2010, "Effect of Surface Roughness on Loss Behaviour, Aerodynamic Loading and Boundary Layer Development of a Low-Pressure Gas Turbine Airfoil," ASME Turbo Expo 2010: Power for Land, Sea, and Air, ASME, pp. 1535–1547.

[23] Montis, M., Niehuis, R., and Fiala, A., 2011, "Aerodynamic Measurements on a Low Pressure Turbine Cascade With Different Levels of Distributed Roughness," ASME 2011 Turbo Expo: Turbine Technical Conference and Exposition, ASMEDC, pp. 457–467.

[24] Zhang, Q., Lee, S. W., and Ligrani, P. M., 2004, "Effects of Surface Roughness and Turbulence Intensity on the Aerodynamic Losses Produced by the Suction Surface of a Simulated Turbine Airfoil," J. Fluids Eng., **126**(2), p. 257.

[25] Zhang, Q., Goodro, M., Ligrani, P. M., Trindade, R., and Sreekanth, S., 2006, "Influence of Surface Roughness on the Aerodynamic Losses of a Turbine Vane," J. Fluids Eng., **128**(3), p. 568.

[26] Kind, R. J., Serjak, P. J., and Abbott, M. W. P., 1998, "Measurements and prediction of the effects of surface roughness on profile

losses and deviation in a turbine cascade," J. Turbomach., **120**(1), pp. 20–27.
[27] Suder, K. L., Chima, R. V., Strazisar, A. J., and Roberts, W. B., 1995, "The Effect of Adding Roughness and Thickness to a Transonic Axial Compressor Rotor," J. Turbomach., **117**(4), pp. 491–505.
[28] Blair, M. F., 1974, "An Experimental Study of Heat Transfer and Film Cooling on Large-Scale Turbine Endwalls," J. Heat Transfer, **96**(4), pp. 524–529.
[29] Blair, M. F., 1994, "An Experimental Study Heat Transfer in a Large-Scale Turbine Rotor Passage," J. Turbomach., **116**(1), pp. 1–13.
[30] Lorenz, M., Schulz, A., and Bauer, H.-J., 2012, "Experimental Study of Surface Roughness Effects on a Turbine Airfoil in a Linear Cascade— Part I: External Heat Transfer," J. Turbomach., **134**(4), p. 041006.
[31] Lutum, E., Cottier, F., Crawford, M. E., Laveau, B., and Abhari, R. S., 2015, "A computational investigation of the effect of surface roughness on heat transfer on the stator endwall of an axial turbine," Proc. Inst. Mech. Eng. Part A J. Power Energy, **229**(5), pp. 454–464.
[32] Guo, S. M., Jones, T. V, Lock, G. D., and Dancer, S. N., 1998, "Computational Prediction of Heat Transfer to Gas Turbine Nozzle Guide Vanes With Roughened Surfaces," J. Turbomach., **120**(2), p. 343.
[33] Samad Power, 2019, "TwinGen" [Online]. Available: http://twingen.co.uk/. [Accessed: 28-Jan-2020].
[34] Menter, F. R., Kuntz, M., and Langtry, R., 2003, "Ten Years of Industrial Experience with the SST Turbulence Model," Turbul. Heat Mass Transf. 4, **4**, pp. 625–632.
[35] Kang, Y.-S., Yoo, J.-C., and Kang, S.-H., 2006, "Numerical predictions of roughness effects on the performance degradation of an axial-turbine stage," J. Mech. Sci. Technol., **20**(7), pp. 1077–1088.
[36] Shabbir, A., and Turner, M. G., 2004, "A Wall Function for Calculating the Skin Friction With Surface Roughness," Volume 5: Turbo Expo 2004, Parts A and B, ASME, pp. 1661–1671.
[37] ANSYS, I., 2013, "ANSYS CFX-Solver Theory Guide."
[38] Adams, T., Grant, C., and Watson, H., 2013, "A Simple Algorithm to Relate Measured Surface Roughness to Equivalent Sand-grain Roughness," Int. J. Mech. Eng. Mechatronics, **1**(1).

Assessment of surface roughness effects on micro axial turbines

Gamil, Abdelaziz A. A.

2021-01-11

Gamil AAA, Nikolaidis T, Teixeira JA, et al., (2021) Assessment of surface roughness effects on micro axial turbines. In: ASME Turbo Expo 2020, 21-25 September 2020, London, Virtual Event. Paper number GT2020-16336

https://doi.org/10.1115/GT2020-16336